Materials Research. 2023; 26(suppl. 1):e20230076
DOI: https://doi.org/10.1590/1980-5373-MR-2023-0076

Copper Binary and Ternary Alloys as Anticorrosive Coatings for Carbon Steel in a Saline Medium

***Thais Machado de Souza*[a], *Gustavo Dionisio Mesquita*[a], *Bruno S. M. Loureiro*[a],**

Lucas Ferreira da Silva Dias*[a], *Dalva C. B. do Lago*[a], *Lilian F. de Senna*[a]

[a]*Universidade do Estado do Rio de Janeiro (UERJ), Instituto de Química, Laboratório de Corrosão e Eletroquímica (LEC), Rua São Francisco Xavier, 524, Pavilhão Haroldo Lisboa da Cunha, S. 427, Maracanã, 20550-013, Rio de Janeiro, RJ, Brasil.*

Received: January 15, 2023; Revised: May 14, 2023; Accepted: June 18, 2023

This work compares the anticorrosive properties of DC electrodeposited CuCoNi, CuCo, and CuNi alloy coatings in a NaCl 0.5 mol L^{-1} solution. The results showed that j and the bath composition influenced the chemical, morphological, and electrochemical characteristics of the alloy coatings. Among all the studied coatings, the CuCo, CuNi, and CuCoNi ones produced at j = 10 A m^{-2}, j = 60 A m^{-2}, and j = 25 A m^{-2}, respectively, showed the best anticorrosive performances in the saline medium, exhibiting charge transfer resistances (R_{tc}) higher than 2000 Ω cm^2 and an electrical double layer capacitances (C_{dl}) lower than 8 X10^{-4} F cm^{-2}. These results agree with the compact morphologies and smaller grain sizes presented by these coatings. Therefore, the anticorrosive properties of the coatings cannot be related only to the less noble metal(s) contents in the alloy but also to their morphologies.

Keywords: *DC electrodeposition, functional coatings, Copper alloys, sodium tartrate, anticorrosive protection.*

1. Introduction

Copper coatings are frequently used as functional coatings for various technical applications due to their excellent electrical and thermal conductivity, high ductility, and corrosion resistance[1,2]. However, the low mechanical resistance of copper, mainly at high temperatures, and the undesirable resistance to wear limit its application[3]. Thus, the production of copper alloy coatings is interesting from an industrial point of view since it confers enhanced properties to the final coating/substrate system.

Functional metallic coatings based on copper alloys showing excellent anticorrosive performances can be produced by DC electroplating[4-10]. This technique permits the control of the deposited materials' properties, and the availability and manipulation of the equipment used to produce the coating are easy[11].

Copper alloys containing cobalt or nickel present improvements in resistance to high temperatures, wear, and corrosion in a saline environment, compared to pure copper plating[8,12,13]. The production of CuCo alloys, both in bulk and in the form of coatings, has increased over time, having different technological applications depending on the cobalt content. Coatings with a high cobalt content can be used for catalytic purposes[14,15] and have excellent anticorrosive properties in seawater[6,7,16]. On the other hand, alloys with lower content of this element deposited on platinum or silicon substrates find applications in data storage systems and as sensors[17,18].

CuNi alloys, when deposited on various substrates such as steel and copper, have excellent corrosion resistance in acidic and basic media and, especially in chloride-containing solutions or seawater[19]. These alloys are widely applied in the construction of ships, pipelines, and other structures related to seawater, and as parts of equipment for chemical processes, such as heat exchangers, pumps, and valves[20,21]. CuNi alloys are ductile and exhibit good mechanical, electrical, optical, and magnetic characteristics[20,22,23].

Although CuCo and CuNi alloy coatings show interesting properties such as magnetic strength, data storage, and corrosion resistance, the ternary CuCoNi alloy may be an even more promising material. As a high-entropy alloy, this ternary alloy may exhibit a significant performance advantage over traditional ones, such as high strength, ductility, corrosion resistance, fatigue, and wear resistance[24]. Several works indicate that inserting one more alloying element enhanced alloy coatings can be produced. It was observed an improvement in the magnetic resistance when producing ternary Cu-alloy coatings of CuCoCr, CuCoFe, CuCoMn, and CuCoNi and that the last alloy presented superior properties concerning the CuCo alloy[25]. Pané et al.[26] studied the electrodeposition of CuCoNi alloy coatings on a glassy carbon substrate and saw an improvement in magnetic resistance compared with CuCo alloys produced under the same conditions. Other works have also shown that CuCoNi alloys improved the magnetic resistance property of the coatings[27-29]. Therefore, although CuCoNi alloy coatings are not currently used in any

*e-mail: lsenna@uerj.br

commercial application, they have shown high potential to be applied as a magnetic sensor and data storage[28].

The Ni content affects the properties of the ternary alloy coatings. Curiotto et al.[29] verified that the magnetic resistance of CuCoNi alloy coatings prepared using melt spinning increased to a Ni content of 5% m/m. Above this value, however, the magnetic resistance worsened. The coating exhibiting a composition of 85 wt.% Cu, 10 wt.% Co, and 5 wt.% Ni presented a higher magnetic resistance when compared to CuCo alloys. It was also shown that the magnetoresistance of electrodeposited CuCoNi alloy coating was improved as the Ni content in the coating increased. In this case, the result was related to forming a more homogeneous surface[27]. It was also verified that introducing low amounts of nickel in films containing Cu and Co changed the crystalline structure, increasing the magnetoresistance property of the CuCoNi coatings. The conditions in which the content of Co + Ni in the coating was between 10 and 30 wt.% produced uniform, smooth and fine-grained surfaces showing improved properties[26].

As the Ni content directly affects the microstructure of high entropy and ferromagnetic alloys, the increase in this parameter also influences the mechanical and anticorrosive properties of these materials. Kuo et al.[30] showed that the increase in Ni content in $CuFeTiZrNi_x$ alloys decreased the hardness, although increased the corrosion resistance of the alloy in a 3.5 wt.% NaCl solution. On the other hand, Dong et al.[31] observed that the increase in Ni content in an $Al_{0.5}CoCrFeNi_x$ alloy led to the formation of a rich-AlNi B2 phase and caused a selective dissolution in an acid medium and oxidation in an alkaline medium. Therefore, the Ni content effects on the anticorrosive performance of these materials depend on the alloy and the aggressive medium. To the best of our knowledge, however, there is no work dealing with the relationship between the Ni content in the electrodeposited CuCoNi coating and the corrosion resistance of the whole coating/substrate system. Also, there are still few works dealing with the anticorrosive performance of this alloy[32].

The electrodeposition of alloy coatings is a more complex process than that of a single metal, as it requires the simultaneous reduction of all metallic ions on the electrode surface. Thus, complexing agents are usually used to approximate the potentials of the metals that constitute the alloy. Cyanide-based baths were widely used to produce copper alloys[33], despite their high toxicity, difficulty in handling, and the need for strict control of solutions and effluent after use. Because of these problems, electrolytic baths based on environmentally friendly complexing agents have been extensively studied. Over the years, baths based on sodium glycinate, sodium citrate, sorbitol, potassium pyrophosphate, or tartrates have been studied, producing coatings on a carbon steel substrate showing anticorrosive performances comparable to those produced from cyanide baths[3,6,7,34-37].

Sodium tartrate has been shown as a promising environmentally friendly complexing agent to produce coatings and reduce the waste treatment steps. It was used both as the only complexing agent, and joined to sodium citrate in a bath to electrodeposit CuNi alloys on a platinum substrate[36]. The presence of the complexing agent in the bath affected the coating composition and morphology. Anticorrosive ZnNi alloys showing excellent corrosion resistance compared to conventional zinc coatings were also electroplated from an alkaline bath containing tartrate and an organic additive[38]. Recently, CuSn and CuCo alloy coatings were produced on carbon steel substrate using sodium tartrate baths, exhibiting smooth morphologies and high anticorrosive performances[10,39]. However, no report concerns using a sodium tartrate bath to produce CuCoNi ternary alloy.

Therefore, based on the previous discussion, binary CuCo and CuNi alloys and ternary CuCoNi alloys were produced by electrodeposition on AISI 1020 steel substrate from sodium tartrate baths. Although this kind of carbon steel is not usually used in aggressive environments, it is widely employed industrially[40]. The effects of the less noble element contents on the phase deposited and the morphology of the coatings were evaluated. This work aims to compare the anticorrosive performance of these coatings/substrate systems and verify if the properties of the electrodeposited CuCoNi alloy coating are superior to those of the binary alloys produced under the same conditions.

2. Experimental Procedures

2.1. Cathodic polarization curves

Galvanostatic cathodic polarization curves of the steel substrate were obtained in the electrolytic baths described in Table 1 at room temperature (25 °C) using an Autolab PGSTAT 302N potentiostat/galvanostat. The potential ranged between the open-circuit potential and -2.00V_{SSE}, using a scan speed of 0.1 mV s^{-1} and bath stirring speed varying between 0 and 400 rpm. A three-electrode system was used in this experiment. The working electrode was an AISI 1020 carbon steel disk (exposed area = 4.9 x 10^{-4} m^2), previously sanded with sandpapers (100 to 600 grit). These electrodes were further degreased in 40 g/L of NaOH + 0.5 g/L of sodium lauryl sulfate solution at 80 °C for 10 minutes. The counter electrode used was a platinum spiral, which was pickled for 1 minute in a 10% v/v HNO_3 and 20% v/v H_2SO_4 solution. Then the working and counter electrodes were washed with

Table 1. Composition, pH, and conductivity of the solutions used in this work.

Solution	$CuSO_4.5H_20$ (mol L^{-1})	$CoSO_4.7H_20$ (mol L^{-1})	$NiSO_4.6H_20$ (mol L^{-1})	$Na_2C_4H_4O_6.4H_2O$ (mol L^{-1})	pH*	Conductivity (mS/cm)
1	0.02	0.1	-	0.5	8.3	11.73
2	0.02	-	0.1	0.5	7.3	13.63
3	0.02	0.05	0.05	0.5	7.1	13.37

*The pH was adjusted using NaOH 4 mol L^{-1}

distilled water and ethyl alcohol and dried with hot air before immersion in the cell. The potential was measured against a saturated mercurous sulfate (SSE) reference electrode.

2.2. Electrodeposition of CuCo, CuNi, and CuCoNi coatings

The electrodeposition of the Cu-alloy coatings applying direct current (DC) was performed using the same cell and electrodes described in Section 2.1, and the solutions presented in Table 1. In this work, results that differed by less than 5% were considered replicates. Considering this point, the coatings were produced in duplicate at 25 °C and using a stirring speed of 300 rpm, chosen from the polarization curves performed for each system (Section 2.1). These curves were also employed to select the current density values (j) used to produce the coatings: 2, 10, 25, 40, 60, 80 A m^{-2}. A theoretical mass of 5 mg was stipulated, calculating, in each case, the time needed for the deposition of the desired alloys, based on Faraday's Law.

The contents of the alloying elements were obtained after dissolving the layers in nitric acid 20% v/v by flame atomic absorption spectrometry (PERKIN-ELMER A ANALYST 300). The deposition efficiency (E_f) was obtained by dividing the total mass of the elements (m_{dep}, in mg), obtained from flame atomic absorption spectrometry, by the theoretical mass (5 mg), as shown in Equation 1.

$$E_f = \frac{m_{dep}}{5} X 100 \quad (1)$$

The content of each metal (wt. % Cu, wt. % Co and wt. % Ni) in the coatings was calculated from Equations 2, 3, and 4 for the CuCo, CuNi, and CuCoNi alloys, respectively.

$$wt.\%_{Me} = \frac{m_{Me}}{mCu + mCo} \quad (2)$$

$$wt.\%_{Me} \frac{m_{Me}}{mCu + mNi} \quad (3)$$

$$wt.\%_{Me} \frac{m_{Me}}{mCu + mCo + mNi} \quad (4)$$

Where Me = Cu, Co, or Ni

The thickness of the coatings (h) was calculated using Equation 5.

$$h = \frac{m_{dep}}{A\rho_c} \quad (5)$$

Where A is the electrode area (4.9 X 10^{-4} m^2), and ρ_c is the coating density (g cm^{-3}), considering the coating composition.

2.3. Characterization of the coatings

2.3.1. Phase analysis

The phase analysis of the coatings was performed using a RIGAKU MINIFLEX II X-ray diffractometer, using a copper source (40 kV voltage and 25 mA current). The 2θ scanning ranged from 10° to 90°, with a step of 0.020°/s.

The grain size was evaluated, in terms of apparent particle diameter (L_{dp}), using Equation 6, in which 2θ is the diffracted angle and β is the full width at the half maximum (FWHM) of the most intense diffraction line of the diffractograms of the deposited alloys. These parameters were obtained by a Gaussian adjustment using the Origin 8.0® software.

$$L_{dp} = \frac{k\lambda}{\beta \cos\theta} \quad (6)$$

Where k is a constant related to the type of crystal structure, and λ is the wavelength of the incident radiation (nm)[41].

2.3.2. Morphology of the coatings

The morphological analysis of the coatings was carried out by scanning electron microscopy (SEM), using a JEOL scanning electron microscope, model JSM G510 LV, under high vacuum conditions, using a SEI detector, a voltage of 20 kV, and different magnifications.

2.3.3. Electrochemical evaluation of the coating/substrate systems

Electrochemical impedance spectroscopy (EIS) experiments were performed in duplicate to verify the corrosion resistance of the coating/substrate systems. The electrolyte used in these tests was a 0.5 mol L^{-1} NaCl solution. In the three-electrode electrochemical cell used in these experiments, the working electrode was the 1020 carbon steel substrate coated with the electrodeposited alloy (CuCo, CuNi, or CuCoNi). The reference electrode was a saturated calomel electrode (ECS), and a platinum spiral acted as the counter-electrode. For comparison, the same experiment was performed using the bare substrate as the working electrode.

The same potentiostat Autolab model PGSTAT302N was used, and the experiments were carried out after stabilizing the system at the open circuit potential (OCP) for around 60 min. The EIS experiments were performed at OCP, using a frequency range of 10^5 Hz to 10^{-3} Hz and an amplitude of 10 mV. The data of the EIS tests were simulated using the equivalent electrical circuits shown in Figure 1 and NOVA

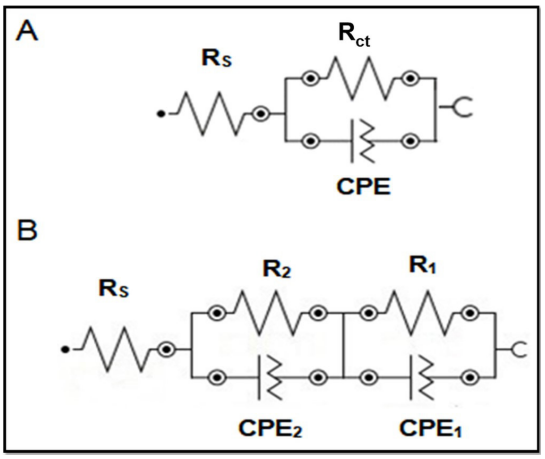

Figure 1. Equivalent circuit models used to simulate EIS data for the studied conditions. (A) carbon steel substrate; (B) CuCo, CoNi, and CuCoNi coating/substrate systems.

1.10 software (Metrohm Autolab). The circuit shown in Figure 1A was used to represent the electrochemical phenomena on the bare substrate surface immersed in the aggressive environment. In this circuit, R_s is the solution resistance, R_{ct} is the charge transfer resistance, and CPE represents the constant phase element associated with the capacitance of the electrical double layer of the substrate. In the circuit of Figure 1B, another time constant is shown, related to the coating, in series with the substrate circuit. Therefore, in this circuit, R_S still represents the solution resistance, and R_1 and R_2 represent the resistance of the substrate and the alloy coating. Similarly, CPE_1 and CPE_2 represent the constant phase element of the substrate and the coating, respectively. In this case, the R_{ct} values was obtained as the summation of R_1 and R_2. The electric double-layer capacitances C_{DL1} and C_{DL2} were calculated based on CPE_1 and CPE_2, respectively, using Equation 7[42]. N_i defines the equivalence degrees of the constant phase elements for each capacitive component obtained in this equation. The final capacitance value (C_{DL}) was obtained using Equation 8.

$$C_{DL_i} = CPE_i^{1/N_i} \times \left(\frac{R_s R_{ct}}{R_s + R_{ct}} \right)^{\left(\frac{1}{N_i} - 1\right)} \quad (7)$$

$$\frac{1}{C_{DL}} = \sum \frac{1}{C_{DL_i}} \quad (8)$$

3. Results and Discussion

3.1. Cathodic polarization curves

Figure 2 shows the cathodic polarization curves of the AISI 1020 carbon steel electrode in each solution presented in Table 1 at different stirring speeds. The cathodic polarization curve tests aimed to select the appropriate current densities used to electrodeposit each alloy (CuCo, CuNi, and CuCoNi) and verify the possible influence of stirring speed on the cathodic processes.

It is noted that all curves show different slopes at various current density regions, which may indicate different deposition modes. At potentials less negative than approximately -0.8 V_{SSE} for CuCo (Figure 2A), -1.0 V_{SSE} for CuNi (Figure 2B), and -0.7 V_{SSE} for CuCoNi (Figure 2C), it is observed a linear region in the polarization curve. This region is probably related to the adsorption of tartrate ions on the substrate, blocking a fraction of the active sites at which the first reduction process (Cu (II) → Cu) takes place[43]. Therefore, the Cu (II) reduction after the Cu-tartrate complex dissociation occurs only on non-blocked active sites. At more negative potentials, the polarization curves exhibit a curved region, revealing the influence of mass transfer processes on the deposition of this metal. In this region, probably, the reduction of Cu (II) ions is controlled by diffusion. For potentials more negative than approximately -1.7 V_{SSE} (Figure 2A) and -1.5 V_{SSE} (Figure 2B), new curved regions

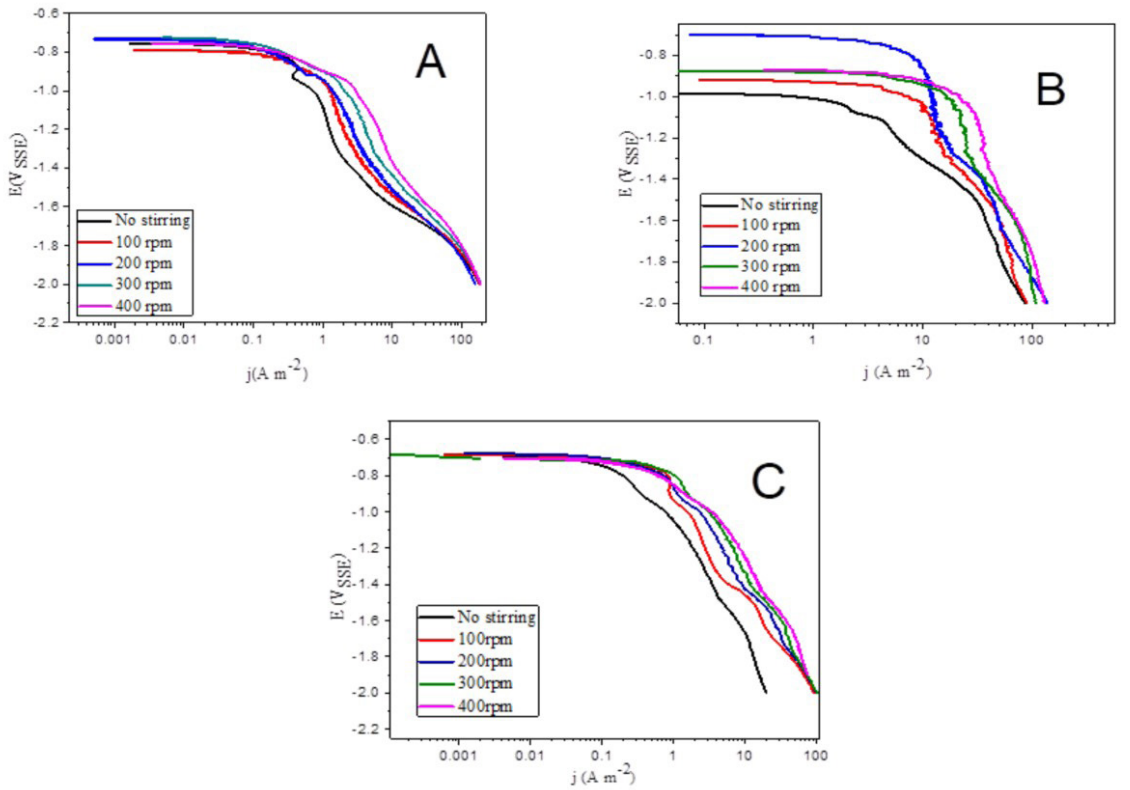

Figure 2. Cathodic polarization curves of carbon steel, obtained under different stirring speeds, in the solutions presented in Table 1. (A) Solution 1 (CuCo alloy coating), (B) Solution 2 (CuNi alloy coating), and (C) Solution 3 (CuCoNi alloy coating).

are observed, probably associated with the reduction of Co (II) and Ni (II) ions, respectively, together with H^+ ions in water. In Figure 2C, two curved regions can be verified at potentials more negative than approximately -1.0 V_{SSE} and -1.5 V_{SSE}, probably associated with the reduction processes of Co (II) and Ni (II) ions, respectively, as the deposition process of these metal ions usually occurs anomalously[27,29,44].

The profile of the polarization curves in Figure 2 also shows a depolarization of the steel electrode as the stirring speed increased, indicating that this parameter seems to influence the electrodeposition processes of the three alloys directly. For the binary CuCo and CuNi alloys (Figures 2A and 2B, respectively), the variation was more pronounced in the region where the reduction of Cu (II) ions is limited by mass transfer. For the ternary CuCoNi alloy (Figure 2C), the whole curves showed variation, and a displacement of the curves towards higher values of current density with increasing stirring speed can be seen. This result suggests that, for the production of the ternary alloy, the solution stirring may interfere with the deposition of the three metals, while in the production of the binary alloys the priority interference is in the copper deposition.

Based on the polarization curves shown in Figure 2, and to avoid turbulence in the fluid during the process, the current densities of 2, 10, 25, 40, 60, and 80 A m^{-2} were selected to produce the alloys, using 300 rpm as the stirring speed.

3.2. Electrodeposition of CuCo, CuNi, and CuCoNi coatings

Table 2 presents the average values of the Cu, Co, and Ni contents in the CuCo, CuNi, and CuCoNi coatings obtained using DC electrodeposition at the selected current density values (Section 3.1). Additionally, average values of the deposition efficiency (E_f) and estimated thickness (h) are presented for each alloy.

In an electrodeposition process, all the applied current is expected to be used to deposit the metallic coating. Unfortunately, a fraction of this current is generally used by some other parallel processes and is considered wasted. Therefore, the current efficiency (E_f), defined as the ratio between the current used in the desired reactions (cations reduction) and the total current applied in the process, is an essential task in the commercial electrodeposition process. Knowing the E_f values permits predicting the period for replacement of chemical reagents, additives, brighteners, levelers, and water softeners in the bath, calculating the content of deposited materials, and verifying the costs of the process.

In the present work, the deposition efficiency values (E_f) varied between 37 and 80%, 41 to 80%, and 15 and 97% for CuCo, CuNi, and CuCoNi, respectively, depending on the current density (j) used for deposition. It was expected that the E_f values for the binary alloys would decrease as the current density increased and, consequently, as the less noble content of metals in the alloy increased. Although this tendency can be noted, this work did not observe a direct relationship among the applied current density, the less noble metal content in the alloy, and the E_f value. In the CuCo alloy, the increase in Co content (wt.% Co) until 10 A m^{-2} elevated the E_f to its maximum value (80%), while further increases in wt.% Co caused a decrease in the cathodic efficiency. The highest E_f value for the CuNi alloys (80%) was also obtained at j = 10 A m^{-2}, where the lowest Ni content in the coating was detected (0.2 wt.% Ni); further increases in wt.% Ni led to a decrease in the E_f values. These results may be probably related to the selected j values, as some values were in the mass transport regions of the curves shown in Figure 2.

In the case of the ternary CuCoNi alloy deposition, the E_f value increased with j up to a maximum value (97%) at j = 25 A m^{-2}, following the increase in wt.% Co in the coating. The further increase in wt.% Co and decrease in wt.% Ni caused a decrease in E_f until j = 60 A m^{-2}. A slight increase in the highest current density value (j = 80 A m^{-2}) was observed, related to a rise in Cu content. Therefore, the coating E_f is related to the deposition of all alloy components, not only to the less noble content in the coating. When the three alloys are compared, the highest E_f value (97%) was obtained for the CuCoNi alloy using j = 25 A m^{-2}, and the lowest E_f value (15%) was verified for the same alloy produced at j = 80 A m^{-2}.

Table 2 also presents the average estimated thickness (h) of the DC-produced coatings. It would be expected that h decreased as j increased, as a function of the decrease in copper content (atomic radius = 128 pm) and an increase in less noble metals cobalt and nickel (atomic radius = 125 pm for both metals). As already verified for E_f values, this relationship was not observed for the alloys studied in the present work. Additionally, it is possible to note that coatings presenting h < 1 μm were deposited in most of the experiments. The h values were calculated using Equation 5, depending on the alloy's density, considering the metallic contents in each deposited coating. Therefore, as the mass

Table 2. Average contents (wt. %Cu, wt. %Co, and wt. %Ni), estimated thickness (h), and deposition efficiency (E_f) of the coatings produced for each alloy.

j (A m^{-2})	CuCo				CuNi				CuCoNi				
	wt.%Cu	wt.%Co	E_f (%)	h (μm)	wt.%Cu	wt.%Ni	E_f (%)	h (μm)	wt.%Cu	wt.%Co	wt.%Ni	E_f (%)	h (μm)
2	96.2	3.8	46	0.52	98.3	1.7	78	0.70	99.8	0.2	-	79	0.90
10	75.6	24.4	80	0.91	99.8	0.2	80	0.91	99.7	0.3	-	93	1.06
25	46.6	53.4	37	0.42	72.5	27.5	53	0.63	60.9	28.3	10.8	97	1.12
40	71.2	28.8	39	0.45	78.2	21.8	66	0.76	53.6	36.9	9.4	75	0.86
60	51.2	48.8	63	0.72	53.9	46.1	62	0.72	59.9	33.7	6.5	15	0.17
80	51.1	48.9	72	0.84	65.1	34.9	41	0.48	66.5	24.4	9.1	25	0.29

values deposited under the conditions of these experiments were low (< 5.0 mg), the low thickness values obtained for all deposited coatings can be considered an expected result. Thus, it is worth noting that both the atomic radii and the deposited mass of the alloy affected the calculated values of h[39]. Among all the studied alloys, the highest thickness value (1.12 μm) was obtained for the CuCoNi alloy, prepared at j = 25 A m^{-2}. It was also the condition where the highest E_f value was found.

The average chemical composition of the coatings (wt. %) for each deposition condition is also shown in Table 2. The values of wt. %Cu were consistently higher than those of wt. % Co and/or wt. % Ni for all the electrodeposited coatings. Furthermore, the cobalt or nickel contents in the CuCo or CuNi coatings were lower than in their respective deposition baths (82.3 wt. % Co and 82.2 wt. % Ni for Solutions 1 and 2, respectively). These results confirm that, for binary alloys, the deposition of the noblest metal (copper) was favored in all the studied conditions, confirming a regular deposition of these alloys[44]. However, the Ni and Co co-deposition processes in the ternary alloy configure an anomalous process, as the Co (II) ions were reduced preferentially to Ni (II) ions. Also, considering the contents of the two metallic ions in the bath (50.1 wt.% and 49.9 wt.% for Co and Ni, respectively, in Solution 3), the cobalt content in the coatings exceeded this proportion in relation to nickel, confirming the anomalous deposition processes between these two metals. This effect has already been reported in other works[26-28].

The anomalous behavior of binary CoNi alloys is well known and several explanations can be related to this process. Sasaki and Talbot[45] proposed that monohydroxides are responsible for anomalous co-deposition. The $Co(OH)^+$ layer would be greater than $Ni(OH)^+$ due to its lower dissociation constant. The anomalous deposition process of Co (II) and Ni (II) can also be based on the concentration gradients on the cathodic surface, similar to the Hessami and Tobias[46] proposal for Fe and Ni deposition. In the present case, this gradient would be more significant for Co (II) than Ni (II) and increases with polarization. Zech et al.[47] suggest that the anomaly of these metallic ions' reduction processes would be related to the kinetics effect of the deposition process. According to the authors, in the potential range where the reduction reactions are under kinetic control, the deposition of the less noble metal inhibits the deposition of the more noble metal. Furthermore, the reaction rate of the less noble metal is catalyzed by the noblest component.

Nonetheless, the bath composition and the current density (or potential range) also influenced the deposition of a binary CoNi alloy[48-50], and both regular and anomalous processes were reported for this alloy deposition. When the alloy was produced from a sulfate bath containing citrate as the complexing agent, anomalous deposition was observed[50]. The present work uses sulfate metallic salts and tartrate (an anion from a carboxylic acid and very similar to citrate) as the complexing agent to produce the coating alloys. As the solutions used are very similar to that studied by[50], an anomalous behavior was likely for the less noble metals in the ternary alloy.

It was expected that at the highest current density studied (80 A m^{-2}), a decrease in the less noble metals' contents and the E_f values could be noted, suggesting that under this condition, part of the applied current may have been consumed by other reactions than the metallic ions reduction[51]. It is known that, during direct current electrodeposition, the reduction of Cu (II), Co (II), and Ni (II) ions is controlled by the continuous consumption of these ions on the substrate surface. After this step, the reduction depends on the transport of these species from the bulk to the substrate surface, which causes a cathodic polarization and improves different parallel reactions. Considering the pH values of the electrolytes (between 7 and 8.3) and the conditions used in the present work (aerated solution), the main parallel reactions occurring at j = 80 A m^{-2} may be the hydrogen evolution reaction (HER, Reaction 1) from water, and the oxygen reduction reaction (ORR, Reaction 2).

$$H_2O + e^- \rightarrow \frac{1}{2}H_2 + OH^- \quad (1)$$

$$2H_2O + O_2 + 4e^- \rightarrow 4OH^- \quad (2)$$

However, the earlier-mentioned effects in the less noble metals contents and E_f values were not observed in the data shown in Table 2. The second highest E_f value for CuCo alloy coating was obtained at 80 A m^{-2}, while the Ni content in the CuNi coating and the Ni and Co contained obtained in the CuCoNi coating obtained under this current density were not the smallest ones among their respective set of experiments. As both parallel reactions presented in Reactions 1 and 2 produce OH^- on the surface/electrolyte interface, the precipitation of cobalt and/or nickel hydroxides could have occurred, contributing to the increase in the less noble metals' content in the alloys.

Nonetheless, the electrode polarization and the parallel reactions occurred during the production of the studied coatings. The effective contribution of each metallic ion in the co-deposition process and that verified for the parallel reactions can be observed by the variation of their respective partial current density (j_{Cu}, j_{Co}, and j_{Ni}) for each potential measured during the electrodeposition of the alloys. Figure 3 shows these results, including the partial current density for the parallel reactions ($j_{parallel}$), obtained as the difference between the total applied current density (j_{total}) and the partial current density for the metals forming each alloy.

It is possible to notice that, independent of the alloy, the j_{Cu} curve is closer to j_{total} than the curves for the less noble metals, mainly at lower j_{total} values, confirming that most of the applied current density was used to reduce the Cu (II) ions. It is also verified that the $j_{parallel}$ curve (related to the parallel reactions) is closer to the j_{total} than the partial curves of the less noble metals at high current density values, mainly for CuNi (Figure 3B) and CuCoNi (Figure 3C) alloys. The small values of j_{Co} and/or j_{Ni} and the high substrate polarization observed in their curves reflect the difficulty of reducing these metals on the steel substrate under the conditions used in this work, even when high current density values were used. These results confirm that the presence of parallel reactions at high j values decreased the amount of applied current used to reduce these metals. Additionally, the anomalous behavior observed for Co and

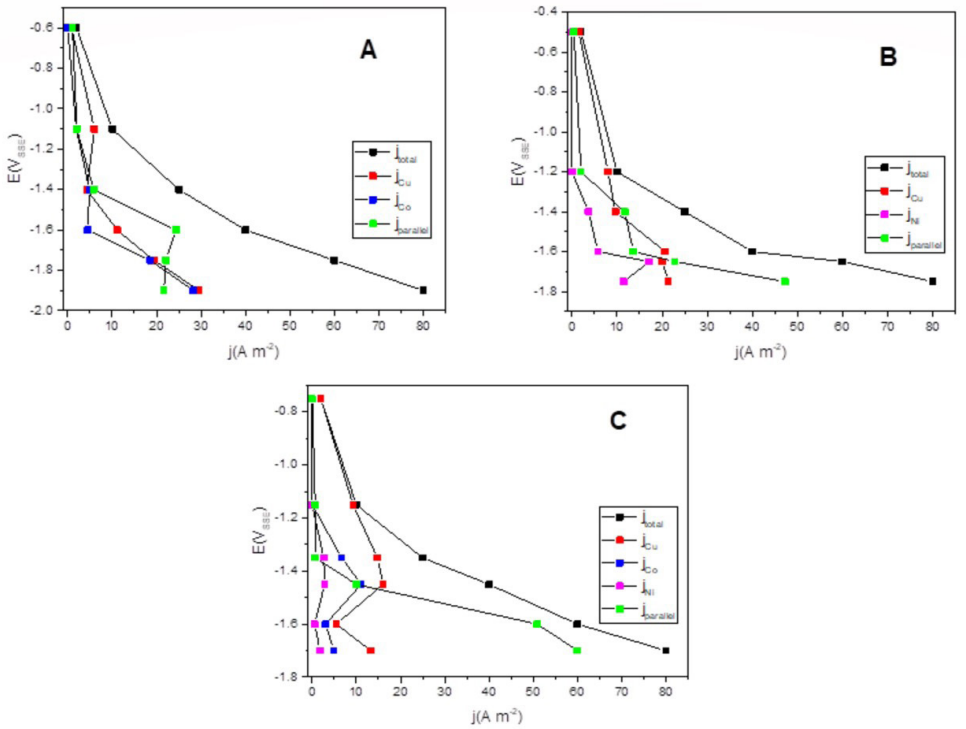

Figure 3. Partial polarization curves showing the current densities (j_{Cu}, j_{Co}, and j_{Ni}) used to reduce each of the metallic ions to produce (A) CuCo alloy coatings; (B) CuNi alloy coatings; and (C) CuCoNi alloy coatings from the solutions of Table 1. The current density used in the parallel processes ($j_{parallel}$) is also shown for comparison.

Ni depositions in CuCoNi alloy is confirmed in Figure 3C, as j_{Co} was always higher than j_{Ni}.

3.3. Characterization of CuCo, CuNi, and CuCoNi coatings

3.3.1. Phase analysis

Figure 4 shows the diffraction lines for CuCo (Figure 4A), CuNi (Figure 4B), and CuCoNi (Figure 4C) alloys deposited on the carbon steel substrate. Electrolytically produced alloy coatings usually consist of thin and non-uniform composition films, presenting a considerable distortion of the crystalline lattice due to the presence of non-equilibrium phases formed in the cathode at high potential values[52]. Therefore, it is generally difficult to analyze these films using the traditional XRD approach, and in some cases, uncatalogued crystalline phases may be obtained.

It is possible to notice in Figure 4 a high-intensity diffraction peak at $2\theta \approx 44.6^{o}$ related to the steel substrate (PDF 06#0696)[53] due to the incidence angle (90^{o}) and other important information concerning the phases observed in each coating. For the CuCo film (Figure 4A), the intense peaks observed in the diffractograms at $2\theta \approx 43.7°$ indicate that this film has a preferential orientation (111)[35,54]. It is known that massive CuCo alloys have an FCC structure at room temperature, a phase rich in copper, with a preferential orientation of planes (111)[55]. Nonetheless, this (111) peak decreases as the applied current density increases, probably related to the decrease in copper content observed for these coatings under these conditions. Broad peaks with low intensity at $2\theta \sim 51.2°$ and $2\theta \sim 75.1°$ are also present in the diffractogram and may be related to orientations (200) and (220), respectively[35,54]. Similar results were found for the CuCo alloy coating produced with citrate and glycine baths with good anticorrosive properties[6,35]. These works correlated the anticorrosive properties observed in the coatings with their (111) preferred orientation. It can also be noted that the diffraction lines observed in the diffractogram of the coating deposited at $j = 80\ A\ m^{-2}$ were mainly related to the substrate steel, which could be due to the small grain size and more amorphous film[56].

An intense peak at $2\theta \sim 43.5°$, with preferential orientation (111) and FCC phase, was found for the CuNi film (Figure 4B), mainly at low current density values (until $j = 25\ A\ m^{-2}$). For the films produced using higher j values, this peak appears as a shoulder in the diffractograms, along with the substrate peak, suggesting a decrease in grain size with current density. Broad and weak peaks were also found at $2\theta \approx 50.5°$ and $2\theta \approx 74.3°$, related to CuNi (200) and (220), respectively, except for $j = 80\ A\ m^{-2}$, where these peaks were not noticeable. Similar results were found in works that produced CuNi alloys by electrodeposition, using different electrolytic baths, salt concentrations, and pH[57-60]. The CuNi coatings produced by Varea et al.[58] and Thurber et al.[60] were electrolytically evaluated and presented high anticorrosive properties in 0.5 mol L^{-1} NaCl medium. However, the authors did not indicate any relationship between the preferential orientation and the anticorrosive performance of the coatings.

Again, only the steel diffraction lines were observed in the diffractogram of the coating produced at j = 80 A m^{-2}, suggesting the presence of a coating with small grain sizes.

The diffractograms of CuCoNi coatings (Figure 4C) show FCC phases and the characteristic diffraction lines (111) (preferred orientation), (200), and (220), observed at 2θ ≈ 43.2, 51.3, and 75.0, respectively. The most crystalline peaks were verified at j = 10 A m^{-2} and 25 A m^{-2}; as the current density increased, these peaks became less intense. Similar diffraction patterns were found for electrodeposited CuCoNi alloy coatings produced in baths containing boric acid and citrate[26,27,29]. Like what was previously mentioned for CuCo and CuNi films, the coating produced at 80 A m^{-2} probably presented small grain, resulting in a diffractogram in which only the substrate peaks were detected.

The experimental 2θ and *d (hkl)* values for the main diffraction lines observed in the diffractograms shown in Figure 4 are presented in Table 3. As a comparison, the standard values *d (hkl)*, corresponding to the phases observed in Figure 4, obtained from the database (Materials Data JADE 5 XRD pattern processing), are also shown in these tables. As these films consist of small crystals and are non-uniform in composition, it is possible that the d (hkl) experimental values are not precisely the same as those found in available databases in most cases.

When analyzing the *d (hkl)* values for the CuCo alloy coatings, CoOOH-related diffraction peaks were recorded at 2θ ≈ 43.7° (140). Jagadale et al.[61] reported the presence of the CoOOH cubic structure in the production of these coatings using potentiostatic electrodeposition. However, the authors used a $CoCl_2$ solution at pH~12, alkalinized with ammonium hydroxide. Under these conditions, the CoOOH could have been precipitated on the substrate. In the present work, the diffraction peak observed at 2θ ≈ 43.7°

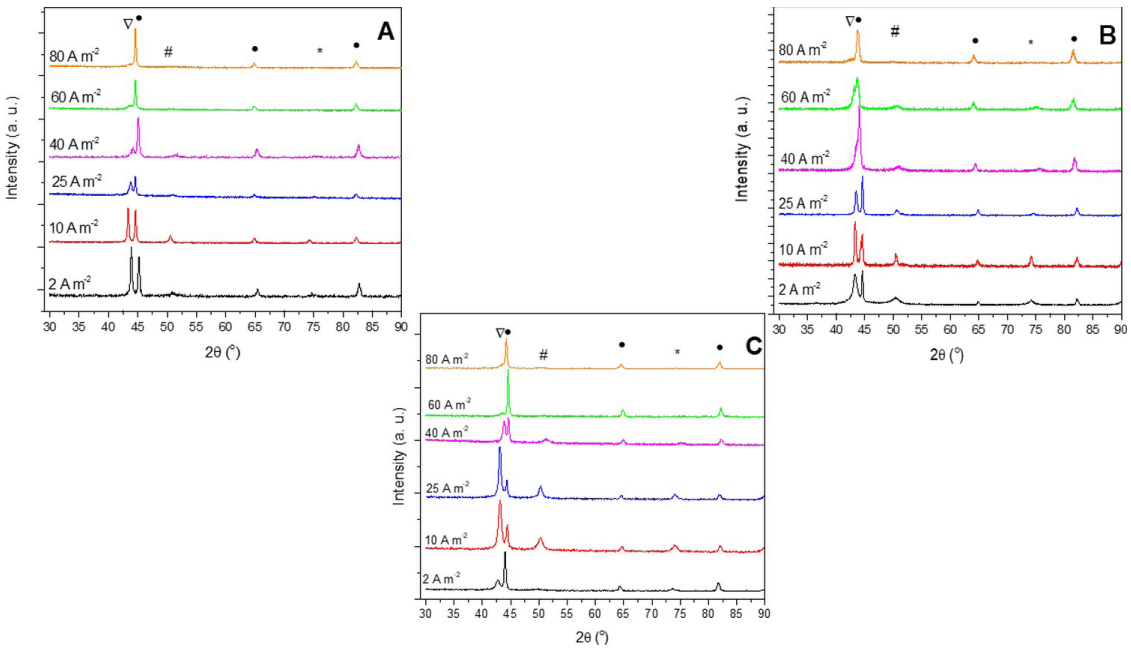

Figure 4. X-ray diffractograms of the coatings produced from the solutions of Table 1 (A) CuCo; (B) CuNi; (C) CuCoNi. Legend: diffraction lines related to the coatings' phases (∇(111), # (200), * (220), % (311)), and those of the Fe from the substrate (•).

Table 3. Average values of *d* (hkl) for CuCo, CuNi, and CuCoNi coatings produced from tartrate bath.

Observed values		Standard values					
2θ (°)	*d* (hkl)	*d* (hkl) carbon steel[a]	*d* (hkl) Cu[b]	*d* (hkl) Co[c]	*d* (hkl) Ni[d]	*d* (hkl) CoOOH[e]	*d* (hkl) $NiCo_2O_4$[f]
43.2 – 43.9	2.09 – 2.06		2.09 (111)	2.03 (111)		2.07 (200)	
44.4 – 45.2	2.04 – 2.00	2.02 (110)		2.03 (111)	2.03 (111)		
50.3 – 51.2	1.78 - 1.81		1.81 (200)		1.76 (200)		
64.8 - 65.6	1.44 – 1.42	1.43 (200)					
74.0 – 74.8	1.28 – 1.27		1.28 (220)	1.25 (110)	1.26 (220)		1.23 (622)
82.0 – 82.9	1.17 – 1.16	1.17 (211)					

[a] PDF#06-0696; [b] PDF#04-0836; [c] PDF#15-0806; [d] PDF#04-0850; [e] PDF#26-480; [f] PDF#10-0188

may be mainly influenced by metallic Co and Cu (PDF#15-0806 and PDF#04-0836, respectively)[53]. The CoOOH cubic structure could be included mainly at high j values due to the OH^- production in the substrate/surface interface due to the parallel reactions occurring during the electrodeposition (Reactions 1 and 2).

While only peaks related to Cu and metallic Ni were observed for the CuNi alloy coatings, it is noted the possible influence of $NiCo_2O_4$ and CoOOH cubic phases in addition to Cu, Co, and metallic Ni for the CuCoNi alloy coatings. The peaks that can be related to the mixed oxide $NiCo_2O_4$ are those present at $2\theta \approx 44.6°$, 64.9°, 75.0° and 82.2° (PDF#10-0188)[53,62,63]. This result can also be associated to the interface alkalization caused by HER and ORR, forming metallic oxides and hydroxides on the electrode surface. The presence of $NiCo_2O_4$ phase in these coatings may agree with the work of Sasaki and Talbot[45], who proposed the formation of a mixed intermediate during the electrodeposition process that favored the deposition of cobalt in relation to nickel, explaining the anomalous deposition in the co-deposition of these metals.

The crystallite sizes for the most intense peak with orientation (111) of CuCo, CuNi, and CuCoNi alloy coatings were obtained from Equation 6, and the results are shown in Table 4. Small grain sizes, on a nanometric scale, were observed for all films produced, ranging from 4 to 25 nm for CuCo films, 4 to 26 nm for CuNi films, and 4 to 16 nm for CuCoNi films. These results agree with those found by Karaagac et al.[64] for CuCo films electroplated using a boric acid bath (≈ 50 nm), Goranova et al.[19], for electrodeposited CuNi alloy coatings from a sodium citrate bath (24 to 40 nm), and Karpuz et al.[27] for CuCoNi coatings produced from a boric acid bath (35 to 64 nm).

It is possible to note a trend to decrease the grain size as the applied current density increased for the CuCo and CuNi films, which may be related to the decrease in the crystallinity of the coating, as seen in Figures 4A and 4B. Crystallization in an electrodeposition process usually involves two steps. The first is linked to the discharge of ions and the generation of atoms from these ions. In the second stage, two scenarios are possible: (1) the incorporation of the atom into the crystal and crystal growth; and (2) the formation of new nuclei when the crystal growth rate is insufficient to generate atoms[65]. It has been proved that the critical surface core radius is a function of excess potential: the higher the potential, the smaller the core radius and the higher the nucleation rates.

Table 4. Apparent grain size (L_{dp}) for CuCo, CuNi, and CuCoNi alloy coatings calculated using Equation 6.

j (A m^{-2})	CuCo	CuNi	CuCoNi
	L_{dp} (nm)	L_{dp} (nm)	L_{dp} (nm)
2	23	7	7
10	25	26	11
25	11	17	16
40	9	10	13
60	4	8	4
80	4	4	5

As the deposition speed increases with j, generating a faster deposition and smaller grains, the formation of new nuclei is expected under the present conditions[17,66]. For the CuCoNi coating, however, there is an increase in grain size until j = 25 A m^2; after this value, the decreasing trend mentioned earlier can be noted.

The decrease of the crystallite size can also be related to decreasing the copper content and the enhancement of cobalt and/or nickel contents in the alloy as j increased. The lowest crystallite values for CuCo and CuNi films (4 nm) were verified at 80 A m^{-2}. Under these conditions, high levels of less noble metals were present in these coatings (48.9 wt.% Co and 34.6 wt.% Ni, for CuCo and CuNi coatings, respectively). For the CuCoNi coatings, however, the crystallite size increases with the cobalt content in the coating until j = 25 A m^{-2}, where the highest nickel content (10.5 wt.% Ni) is also present. Further, an increase in wt.% Co and a decrease in wt.% Ni led to a decrease in grain size. The smallest grain size values were obtained at j = 60 A m^{-2} (4 nm) and j = 80 A m^{-2} (5 nm), where the contents of the less noble metal were, respectively, wt.% Co = 33.7 and wt.% Ni = 6.5, and wt.% Co = 24.4 and wt.% Ni = 9.1.

3.3.2. Morphological evaluation

The micrographs obtained for the surfaces of the CuCo, CuNi, and CuCoNi alloy coatings are shown in Figure 5 (magnification of 5000 X), and the homogeneity, shape, and size of the formed grains and agglomerates can be observed. In this figure, the CuCo, CuNi, and CuCoNi films are designated as 1, 2, and 3, respectively. The differences in the scanning electron microscopy results suggest that the current density and bath composition influenced the coatings produced.

It is possible to note different grain/agglomerate morphologies and sizes when the same current density was applied to produce the coatings using the different solutions presented in Table 1. Independently of the evaluated coating, all the substrates were entirely covered during the electrodeposition process. Most coatings show homogeneous surfaces without cracks or defects, presenting globular clusters distributed all over the surface, which may contribute to adequate anticorrosive performance. These characteristics may be related to the leveling action of the tartrate when adsorbed to the substrate surface[33]. However, there are defective coatings, and different agglomerates on their surfaces can be noted.

While a tendency for decreasing the grain size as the current density increases for the CuCo coatings can be noted, this behavior was only observed for the CuNi alloy coatings after an increase from j = 2 A m^{-2} to 10 A m^{-2} under the studied conditions. On the other hand, the CuCoNi coatings' grain sizes tend to increase until j = 25 A m^{-2}, decreasing after this value. These results agree with those verified for the XRD analysis. Among the coatings studied, the CuCo (at high j values) and the CuCoNi ones presented the smallest grain sizes and agglomerates, which may be related to the increase in cobalt content and the presence of both cobalt and nickel in these coatings, contributing to the homogeneity of the formed films. According to Gómez et al.[49], the incorporation

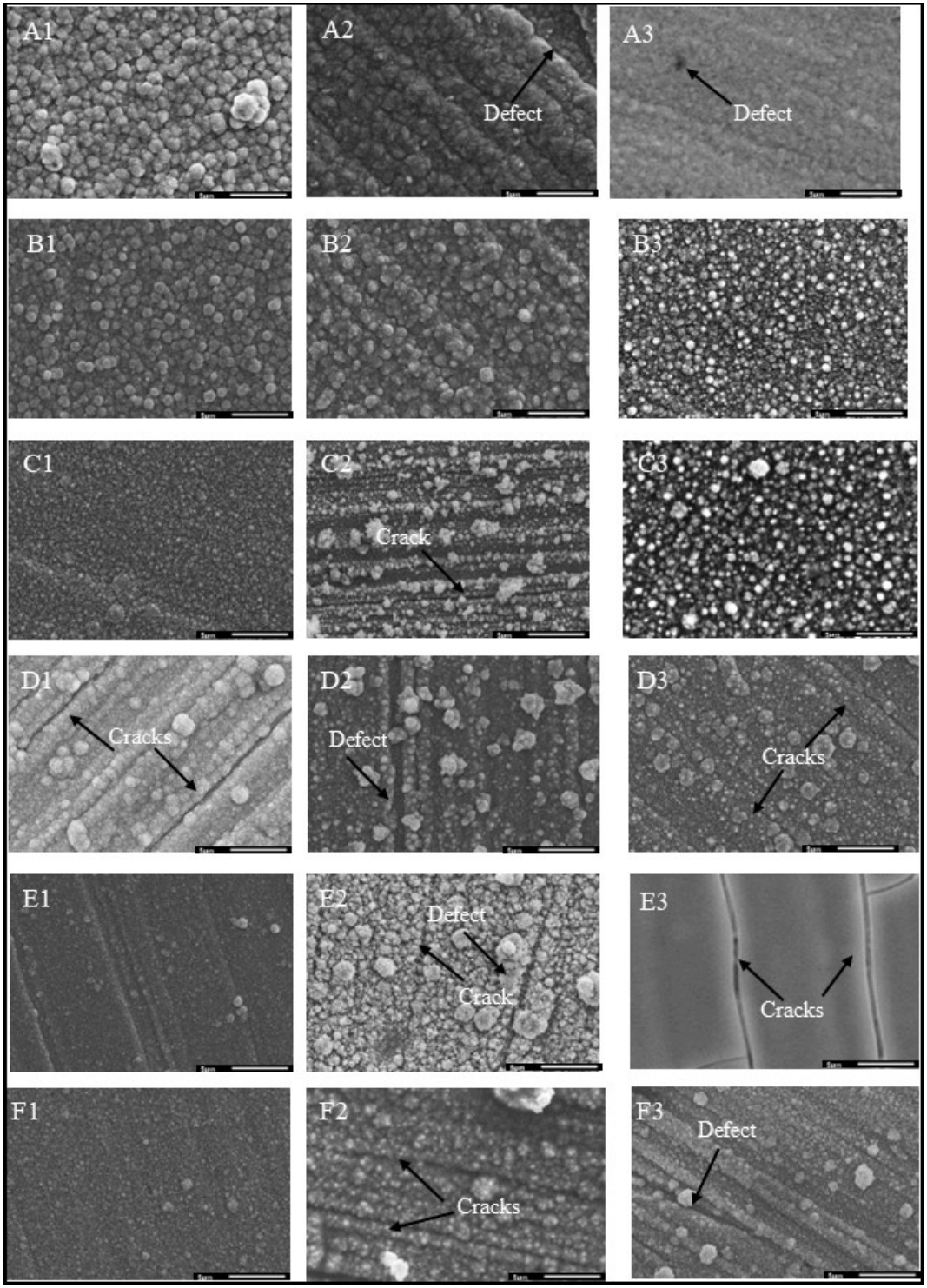

Figure 5. Surface micrographs of the CuCo (1), CuNi (2), and CuCoNi (3) alloy coatings, produced using (A) j = 2 A m^{-2}; (B) j = 10 A m^{-2}; (C) j = 25 A m^{-2}; (D) j = 40 A m^{-2}; (E) j = 60 A m^{-2}; (F) j = 80 A m^{-2} (5,000 X magnification).

of ferromagnetic metals and the increase in nucleation at high potential values involve a decrease in crystal size, leading to uniformity of deposits. Budi et al.[51] noticed that the increase in j improved the homogeneity of the CuCoNi alloy surfaces, although the grain size did not decrease significantly.

The main differences can be noted when the CuCo, CuNi, and CuCoNi coatings are compared for each j value. The CuCo coating produced at j = 2 A m^{-2} (Figure 5A1) presents clusters with a cauliflower-like morphology. Similar morphology has already been observed for copper and different

copper-alloy coatings in the literature[3,10,26]. The CuNi and CuCoNi coatings produced at the same current density value (Figures 5A2 and 5A3, respectively) were more compact and homogeneous, apparently formed by large agglomerates of small and nodular grains. However, the CuCoNi coating shows minor defects over its surface, which could hinder its protection ability in aggressive media. The coatings produced under this j value were mainly composed of copper.

The coatings produced using j = 10 A m^{-2} (Figures 5B) show clusters with apparently rounded grains independent of the copper alloy deposited. A more regular topography can be seen, and compact films were produced. This type of grain is highly orientated and shows well-defined contours. In agreement with the XRD analyses, the smallest grain size obtained under this condition was observed for the CuCoNi coating (Figure 5B3). It is interesting to note that although similar morphologies were obtained, the CuCo coating presents 24.4 wt.% Co, while the CuNi and CuCoNi coatings were mainly composed of copper.

When the coatings' surfaces are compared, an increase in the grain sizes was observed, mainly in Figures 5A2/5B2 and Figures 5A3/5B3 (when increasing from j = 2 A m^2 to j = 10 A m^2), for CuNi and CuCoNi coatings, respectively. It is interesting to remember that, at j = 2 A m^2, the polarization curves presented in Figure 2 show a linear region (principally for the CuNi alloy in Figure 2B), which can be related to the adsorbed tartrate ions that are likely blocking the metallic reduction processes[43] and leading to small amounts of deposited mass. Consequently, low thickness and cathodic efficiency values were observed for these coatings (Table 2), producing surfaces with small grain sizes. Therefore, knowing that thin films are often found to have small grain sizes and considering the rise in the deposited mass achieved when j was increased from 2 to 10 A m^2 (which is reflected in the increase in E_f and h values under these conditions), it is possible to conclude that thinner CuNi and CuCoNi films, exhibiting smaller grain sizes, were probably produced at j = 2 A m^2 when compared to those prepared at j = 10 A m^2.

Nonetheless, there is almost no difference between the E_f values of CuNi and CuCoNi coatings at j = 2 A m^2, although the thickness of the ternary alloy is higher under the same conditions (Table 2). Considering the composition of both alloys, the higher copper content in the CuCoNi coating, when compared to the CuNi alloys, could have led to this difference. Additionally, for the ternary alloy, copper reduction at j = 10 A m^{-2} is controlled by mass transport (Figure 2C), which could have contributed to the changes observed in the coating morphology (Figures 5A3/5B3).

At j = 25 A m^{-2} (Figures 5C), similar morphologies were obtained for the three coatings, although the presence of polyhedral agglomerates on the CuNi coating surface (Figure 5C2) can be noted. These agglomerates could be related to the formation of oxides on the surface due to the parallel reactions and interface alkalization (Reactions 1 and 2). However, the presence of nickel or copper oxides was not detected in the XRD analysis. Minor defects were verified on the CuCo and CuNi surfaces (Figures 5C1 and 5C2, respectively). Under this condition, the CuCo, CuNi, and CuCoNi alloy coatings were produced, showing high contents of the less noble metals. While the grain sizes seem to decrease when j = 40 A m^{-2} was applied to produce all the studied coatings, the size of the agglomerates increased (Figures 5D). Flower-like agglomerates can be observed on the CuNi and CuCoNi coating surfaces (Figures 5D2 and 5D3, respectively) produced using this current density value, which may agree with the presence of oxides on the coatings' surface. Some cracks and defects can also be observed on the coatings' surfaces.

In agreement with the XRD results (Table 5), while the grain size of the CuCo and CuNi coatings decreased at j = 25 A m^{-2}, there was an increase in the grain size of the CuCoNi coating. When the E_f and h values of the coatings under this condition are evaluated (Table 2), it is possible to verify that these parameters also decreased for the CuCo and CuNi coatings and increased for the CuCoNi one, showing their highest values when j = 25 A m^{-2}. Based on the current efficiency definition (Section 3.2), low E_f values can be related to parallel reactions occurring on the cathodic surface apart from the metal deposition. As has already been mentioned, under the conditions used in this work, the main parallel reactions are HER and ORR (Reactions 1 and 2). Therefore, the hydrogen and oxygen reduction processes compete with the reduction of metallic ions.

The effects of these parallel reactions on the deposited mass and the E_f values of the coatings prepared at j = 25 A m^{-2} can be better evaluated in Figure 3, where the partial polarization curves are presented. It can be noted that, under this condition, the current spent in the parallel reactions ($j_{parallel}$) is higher than that used to deposit copper (j_{Cu}) and the less noble metals (j_{Co} or j_{Ni}) in the CuCo and CuNi coatings deposition processes (Figures 3A and 3B, respectively). Also, $j_{parallel}$ increased for higher values of applied current density, meanly for the CuNi coatings. It means that, from j = 25 A m^{-2} on, HER and OER overpowered the metal deposition, decreased the deposited mass, and consequently, the E_f and h values of these coatings. The combined effect of presenting higher contents of less noble metals and lower h values may have contributed to the decrease in the grain size observed for these coatings.

On the other hand, unlike the coatings produced using smaller current density values, both Ni and Co are present in the CuCoNi coating produced at j = 25 A m^{-2}. Figure 3C shows that the $j_{parallel}$ value in the deposition process at this current density is smaller than those verified for j_{Cu}, j_{Co}, and j_{Ni}. It confirms that the deposition of the metals was the main process under this condition, which may explain the high E_f and h values obtained for this coating. Therefore, the CuCoNi coating prepared under this condition presented the highest E_f and h values among all the coatings produced. Although a high cobalt content usually shows a refining effect concerning the grain size of the coating[39], it is likely that the increase in the coating thickness also contributed to the small increase in the grain size observed for this coating. Figure 3C also shows that $j_{parallel}$ increased at 40 A m^{-2} and was higher than the j_{Ni} value, in agreement with the decrease in the E_f and h values (Table 2) and the decrease in the grain size observed for the CuCoNi coatings produced from this current density onwards.

Tiny grains can be noted on the surfaces of the coatings produced using j = 60 A m^{-2} (Figures 5E). It is not possible

to verify the grains or agglomerates on the CuCoNi surface (Figure 5E3), although some agglomerates are present on the CuCo (Figure 5E1) and, mainly, the CuNi surfaces (Figure 5E2). It must be reminded that, under this condition, the smallest E_f (15%) and thickness (0.17 µm) values were verified for the CuCoNi coating. Therefore, this result may also be related to the low thickness of the coating. Cracks can be observed, mainly on the CuNi and CuCoNi surfaces. At j = 80 A m^{-2} (Figures 5F), small grain sizes and several agglomerates continue to be observed on the coatings' surface. Cracks are also noted on the CuNi and CuCoNi surfaces (Figures 5F2 and 5F3, respectively.

3.3.3. Electrochemical evaluation

The anticorrosive performance of the CuCo, CuNi, and CuCoNi coatings was evaluated in 0.5 mol L^{-1} NaCl medium by electrochemical impedance spectroscopy (EIS) analysis. The Nyquist diagrams of the uncoated carbon steel substrate and the prepared coating/substrate systems for each alloy are shown in Figure 6.

In the Nyquist diagrams, the diameters of the capacitive loops can be considered an indication of the corrosion resistance of the coating/substrate system in the aggressive medium. Therefore, it is possible to notice, in Figure 6A, that the CuCo coating prepared at j = 10 A m^{-2}, j = 25 A m^{-2}, j = 60 A m^{-2}, and j = 80 A m^{-2} improved the anticorrosive performance of the substrate in the aggressive medium, showing capacitive loops higher to that of bare carbon steel. These coatings present cobalt content ≥ 24.4 wt% Co, uniform morphologies, and minor defects, which agrees with the literature reports that high anticorrosive CuCo coatings presented high Co contents[7,16,39]. On the other hand, capacitive loops diameters of the systems produced under the conditions of j = 2 A m^{-2} and j = 40 A m^{-2} were smaller than that of uncoated carbon steel, thus favoring the corrosion of the substrate. The coating produced using j = 2 A m^{-2} presented low cobalt content (3.8 wt.% Co) and a loose morphology (Figure 5A1), which could have permitted the substrate attack by the electrolyte and contributed to its low anticorrosive performance. Despite its high cobalt content, the coating prepared using j = 40 A m^{-2} showed cracks on its surface (Figure 5D1), which probably allowed the attack of the substrate by the electrolyte, decreasing the protective ability of this coating and causing localized corrosion.

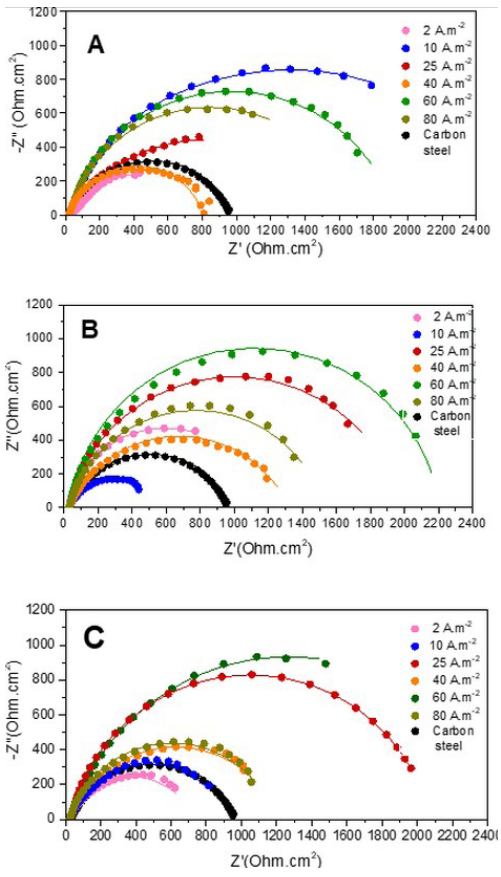

Figure 6. Nyquist diagrams for the (A) CuCo, (B) CuNi, and (C) CuCoNi coating/substrate systems in NaCl 0.5 mol L^{-1} medium. The bare carbon substrate diagram is also shown for comparison.

It is possible to observe for the CuNi alloy (Figure 6B) that only the coating/substrate system produced under the condition of j = 10 A m^{-2} did not show the ability to protect the steel substrate in the studied corrosive medium, as its capacitive loop is lower than that of the bare carbon steel. Despite showing an apparent compact morphology (Figure 5B2), this coating presented the lowest nickel content (0.2 wt %) among those studied for this alloy, which could have contributed to this result. High Ni contents improved the anticorrosive ability of the CuNi coating/substrate systems, confirming that the content of this metal seems to influence the anticorrosive performance of the system[58,60,67]. The system prepared using j = 60 A m^{-2} presented the best anticorrosive performance among all the CuNi coatings produced. This coating showed the highest nickel content (46.1 wt.%) and a compact morphology (Figure 5E2), although some defects can be noted.

In the case of CuCoNi alloy coatings (Figure 6C), only the coating/substrate systems produced under the conditions j = 2 A m^{-2} and j = 10 A m^{-2} showed low anticorrosive performance, as their capacitive loops are smaller than that of the uncoated substrate. Table 2 shows that coatings mainly composed of copper were obtained under these conditions, which can be related to the poor results verified for these systems. Although Figure 5A3 shows that a compact layer was produced, minor defects can also be noted on the surface, decreasing its protection, and contributing to the small Nyquist loop shown by this sample. Among the CuCoNi coatings that improved substrate protection, those produced at j = 25 A m^{-2} and j = 60 A m^{-2} presented the highest anticorrosive performances. These coatings showed Co + Ni content ≈ 40 wt.%, although the increase in j caused an increase in Co and a decrease in Ni contents in the coatings. The literature suggests that the Ni contents' increase in Ni-contain ternary alloys improves the corrosion resistance of the coating[26,58]. Nonetheless, this parameter did not apparently affect the anticorrosive performance of the coating prepared at j = 60 A m^{-2}. Uniform surface morphologies were also found for both coatings (Figures 5C3 and 5E3 for j = 25 A m^{-2} and j = 60 A m^{-2}, respectively), although some cracks are present in Figure 5E3.

The data obtained from the Nyquist diagrams for all the coatings produced were simulated using the equivalent circuit shown in Figure 1B, while the bare substrate was simulated with the circuit presented in Figure 1A. The fitting curves are presented as the solid lines in Figure 6, and the values of R_s, R_{ct} and C_{DL}, obtained from the fitting and Equations 7 and 8, are exhibited in Table 5. This table also presents the fitting error (χ^2), always ≤ 5%. It is usually considered that coatings showing anticorrosive characteristics exhibit high R_{ct} and low C_{DL} values[68]. A high R_{ct} value indicates improved corrosion resistance, while a low C_{DL} value suggests a low tendency to conduct charges[69].

Confirming the results shown in Figure 6A, it is noted that among the CuCo coating/substrate systems prepared using DC electrodeposition, only those produced at j = 2 A m^{-2} and j = 40 Am^{-2} could not protect the substrate, as both systems showed R_{ct} values (590 Ω cm^2 and 847 Ω cm^2, respectively) lower than that of the substrate (960 Ω cm^2). These results agree with the micrographs of these coatings (Figures 5A1 and 5D1), where some defects could be noted. Also, the wt.% Co in the coating produced using j = 2 A m^{-2} was very low (3.8 wt.%). On the other hand, all the other CuCo coatings presented higher R_{ct} and lower C_{DL} values compared to those exhibited by the bare steel, which is also coherent to the compact coatings showing few defects and small grain/agglomerate sizes (Figures 5B1, 5C1, 5E1, and 5F1). These results also confirm those reporting that anticorrosive CuCo coatings showing high wt.% Co can be produced by DC electrodeposition[7,16,39]. Among these systems, it can be noted that the one produced at j = 10 A m^{-2} presented the highest R_{ct} (2560 Ω cm^2) and the lowest C_{DL} (3.50 X 10^{-4} F cm^{-2}) values, therefore being considered the best anticorrosive CuCo coating in NaCl 0.5 mol L^{-1} medium.

The results for the CuNi alloy coatings/substrate systems, also shown in Table 5, confirm the Nyquist diagrams verified in Figure 6B. All the CuNi/substrate coating systems behaved by improving the substrate resistance in the aggressive medium, exhibiting R_{ct} values higher than that verified for the uncoated carbon steel substrate. The only exception was observed for the system produced at j = 10 A m^{-2}, which showed lower R_{ct} (519 Ω cm^2) and higher C_{DL} (1.83 X 10^{-3} F cm^{-2}) values than those of the steel substrate. This coating presented the lowest wt.% Ni value (0.2 wt.% Ni), which could have contributed to its low anticorrosive performance. Although presenting a higher R_{ct} value (1231 Ω cm^2) than that observed for the substrate, the system produced using j = 2 A m^{-2} exhibited a higher C_{DL} value (4.79 X 10^{-3} F cm^{-2}) than that of the bare steel (1.59 X 10^{-3} F cm^{-2}), suggesting that this coating may have a high tendency to conduct the charge. Despite its compact appearance, the surface of this coating shows defects (Figure 5A2), which may have favored the attack of the substrate by the electrolyte, generating conductive corrosion products[70]. Among the CuNi alloy coatings/substrate systems studied, the best anticorrosive performance was verified for that produced using j = 60 A m^{-2}, which exhibited the highest R_{ct} value (2162 Ω cm^2), low grain size (Table 4 and Figure 5E2), and the highest Ni content in the coating (46.1 wt.% Ni). However, this film also shows defects, which could have permitted the aggressive medium to attack the substrate, causing an increase in its C_{DL} value (7.49 X 10^{-4} F cm^{-2}) compared to other systems. Nonetheless, even though this system did not show the smallest C_{DL} value, it was smaller than the substrate C_{DL}.

Considering the CuCoNi alloy coating/substrate systems, Table 5 shows that those coatings produced using j = 2 A m^{-2} and j = 10 A m^{-2} could not be used as protective coatings for steel substrate in a saline medium since their R_{ct} and C_{DL} values were higher and lower, respectively, than those shown for the uncoated substrate. These coatings presented low contents of less noble metals, and, despite their apparent compact morphologies, minor defects can be noted on their surfaces (Figures 5A3 and 5B3, respectively). These coatings tend to behave similarly to those containing low cobalt or nickel contents earlier mentioned, favoring the corrosion of the system. As previously verified in Figure 6C, all the other systems improved the anticorrosive performance of the substrate in NaCl 0.5 mol L^{-1}. The presence of both less noble elements in the CuCoNi alloy coating composition may have contributed to the behavior shown by these systems. However, the systems produced at j = 40 A m^{-2} and j = 80 A m^{-2} presented C_{DL} values (2.12 X 10^{-3} F cm^{-2} and 2.14 X 10^{-3} F cm^{-2}, respectively) higher than that of the steel substrate. Despite their small grain size and compact morphologies, these coatings exhibited cracks on their surfaces, which could have permitted the corrosion of the

Table 5. Values of R_s, R_{ct}, C_{DL}, and χ^2 obtained from the simulation of EIS data for the bare carbon steel and CuCo, CuNi, and CuCoNi coating/substrate systems in NaCl 0.5 mol L^{-1}.

j (A m^{-2})	CuCo				CuNi				CuCoNi			
	R_s (Ω)	R_{ct} (Ω cm^2)	C_{DL} (F cm^{-2})	χ^2	R_s (Ω)	R_{ct} (Ω cm^2)	C_{DL} (F cm^{-2})	χ^2	R_s (Ω)	R_{ct} (Ω cm^2)	C_{DL} (F cm^{-2})	χ^2
2	5.77	590	1.24X10^{-3}	0.04	6.01	1231	4.79X10^{-3}	0.01	5.47	766	3.90X10^{-3}	0.02
10	6.40	2558	3.50X10^{-4}	0.002	6.00	519	1.83X10^{-3}	0.05	5.25	873	7.16X10^{-3}	0.05
25	6.49	1499	4.78X10^{-4}	0.02	6.20	2098	6.34X10^{-4}	0.03	5.64	2102	5.42X10^{-4}	0.05
40	4.50	847	1.22X10^{-3}	0.03	6.20	1334	2.07X10^{-4}	0.05	6.19	1245	2.12X10^{-3}	0.006
60	6.29	1847	4.05X10^{-4}	0.02	5.56	2162	7.40X10^{-4}	0.04	6.15	2160	1.49X10^{-3}	0.04
80	6.14	1456	9.32X10^{-4}	0.04	5.70	1460	2.07X10^{-3}	0.05	4.72	1152	2.14X10^{-3}	0.04
Steel substrate	**R_s (Ω)**				**R_{ct} (Ω cm^2)**				**C_{DL} (F cm^{-2})**			**χ^2**
	6.31				960				1.59X10^{-3}			0.01

substrate and the production of conductive corrosion products on their surfaces[70].

The CuCoNi coating/substrate systems produced using $j = 25\ A\ m^{-2}$ and $j = 60\ A\ m^{-2}$ exhibited the highest values of R_{ct} (2102 Ω cm^2 and 2160 Ω cm^2, respectively) and lowest C_{DL} values (5.42 X 10^{-4} F cm^{-2} and 1.49 X 10^{-3}, respectively). Pané et al.[26] produced anticorrosive alloy coatings containing Ni + Co contents between 10 and 30 wt.% In the present study, these selected anticorrosive coatings show approximately 40 wt. % Co + Ni, which may have contributed to their anticorrosive performance. When these two systems are compared, it is noted that C_{DL} value of that prepared using $j = 60\ A\ m^{-2}$ is near the substrate value. It is essential to remind that this coating presented the lowest thickness and current efficiency values (0.17 µm and 15%, respectively) among all the films deposited and that cracks could be noted on its surface (Figure 5E3), which can be reflected in its high C_{DL} value. On the other hand, the system produced under the conditions of $j = 25\ A\ m^{-2}$ presented a similar R_{ct} value and a lower C_{DL} value compared to that deposited at $j = 60\ A\ m^{-2}$. In addition to presenting high E_f and h values (97% and 1.12 µm, respectively), this coating exhibited a compact morphology (Figure 5C3) with no defects, and a small grain size, which may permit this system to be selected as the best anticorrosive system among the CuCoNi coating/substrate systems prepared from the tartrate bath.

When the selected CuCo ($j = 10\ A\ m^{-2}$), CuNi ($j = 60\ A\ m^{-2}$), and CuCoNi ($j = 25\ A\ m^{-2}$) coating/substrate systems are compared (Figure 7), it is noted that, although a decrease in the grain size and a more compact coating was obtained, the CuCoNi produced from tartrate bath did not enhance the anticorrosive performance of the CuCo and CuNi binary coatings significantly. The ternary coating presented a similar cobalt content of the CuCo coating (24.4 wt.% Co and 28.3 wt.% Co, for the CuCo and CuCoNi coatings, respectively) and a lower nickel content than the CuNi coating (46.1 wt.% Ni and 10.8 wt.% Ni, for the CuNi and CuCoNi coatings, respectively). Likely, a higher Ni content could have improved the quality of this ternary coating, although this result was not obtained under the conditions used in the present study. Therefore, concerning the charge transfer resistance (R_{ct}) and double layer capacitance (C_{dl}) values, all the coatings presented similar performances, and the selected systems could adequately protect the steel substrate in a saline medium. Among them, the CuCo coating produced at $10\ A\ m^{-2}$ showed the highest R_{ct} and smallest C_{dl} values and could be considered the most protective coating produced under the conditions of this work. Nonetheless, based on the E_f values and considering that the barrier effect of this coating may also contribute to protecting the substrate in an aggressive environment, the selected CuCoNi coating, produced at $j = 25\ A\ m^{-2}$, must also be considered an efficient anticorrosive coating. Based on these results, the selected CuCo and CuCoNi coatings stand out and can be considered promising candidates for commercial applications.

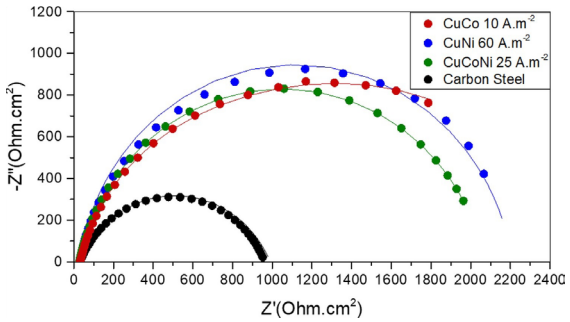

Figure 7. Nyquist diagrams for the selected CuCo, CuNi, and CuCoNi coating/substrate systems that showed the best anticorrosive performances in NaCl 0.5 mol L^{-1} medium.

4. Conclusions

Anticorrosive CuCo, CuNi, and CuCoNi coatings were produced by DC electrodeposition from a tartrate bath. E_f values varying from 15% to 97% were obtained in the production of these coatings, confirming that parallel reactions (HER and OER) are present in their deposition processes, mainly at higher current density values.

Although Co-rich and Ni-rich binary coatings were produced, their morphology and grain sizes also contributed to the anticorrosive performance of these coatings. Co+Ni-rich CuCoNi alloy coatings were obtained, mainly at higher j values. An anomalous deposition process for the Co and Ni deposition was observed, and the cobalt content in these coatings was higher than that observed for the Ni. These ternary coatings exhibited smaller grain sizes and more compact morphologies than the binary alloys, although defects are also present.

The effects of the applied current density and the deposition bath were observed in the cathodic efficiency, thickness, chemical composition, and morphology of the coatings, leading to different electrochemical behaviors in the aggressive medium. The best anticorrosive coatings were obtained using $j = 10\ A\ m^{-2}$, $j = 60\ A\ m^{-2}$, and $j = 25\ A\ m^{-2}$ for CuCo, CuNi, and CuCoNi coating/substrate systems, respectively. These coatings presented high levels of less noble metals in their composition, high E_f values (mainly for the CuCo and CuCoNi coatings), and compacted morphologies, showing minor defects and small grain sizes. Concerning the R_{ct} and C_{dl} values, their anticorrosive performances were similar, and the ternary coating did not improve the corrosion protection of the steel substrate in the saline medium, as expected. However, the high E_f values of the CuCoNi coating may have contributed to enhancing the barrier effect of this coating. Therefore, although both binary (CuCo and CuNi) and ternary (CuCoNi) coatings may be used to protect carbon steel in a NaCl 0.5 mol L^{-1} medium, the present results indicate that the selected CuCo and CuCoNi coatings may be tested commercially as protective coatings.

5. Acknowledgements

This study was financed in part by the "Coordenação de Aperfeiçoamento de Pessoal de Nível Superior - Brasil (CAPES)" - Finance Code 001. The authors would also like to thank the Rio de Janeiro Research Foundation (FAPERJ), the Brazilian National Research Council (CNPq), the State University of Rio de Janeiro (UERJ), and the Prociência Program for financial support. Additionally, we would like

to thank Diego Barros (LEAMS/UERJ) for the chemical analysis and Jessica Pereira Machado (LabMEV/UERJ) for the surface SEM analysis.

6. References

1. Sknar IV, Sknar YE, Savchuk OO, Baskevich AS, Kozhura OV, Hrydnieva TV. Electrodeposition of copper from methanesulphonate electrolyte. J Chem Technol. 2020;28(1):1-9.
2. Pardo A, Merino MC, Coy AE, Arrabal R, Viejo F, M'hich A. Corrosion behaviour of AISI 304 stainless steel with Cu coatings in H_2SO_4. Appl Surf Sci. 2007;253:9164-76.
3. Kaiser S, Kaiser MS. A comparative study of chemical and physical properties of copper and copper alloys affected by acidic, alkaline and saline environments. J Electrochem Sci Eng. 2020;10(4):373-84.
4. Senna LF, Díaz SL, Sathler L. Electrodeposition of copper-zinc alloys in pyrophosphate-based electrolytes. J Appl Electrochem. 2003;33(12):1155-1161.
5. Ferreira FBA, Silva FLG, Luna AS, do Lago DCB, Senna LF. Response surface modeling and optimization to study the influence of deposition parameters on the electrodeposition of Cu–Zn alloys in citrate medium. J Appl Electrochem. 2007;37(4):473-81.
6. de Farias LT, Luna AS, do Lago DCB, Senna LF. Influence of cathodic current density and mechanical stirring on the electrodeposition of Cu-Co alloys in citrate bath. Mater Res. 2008;11(1):1-9.
7. Silva FLG, Garcia JR, Cruz VGM, Luna AS, do Lago DCB, Senna LF. Response surface analysis to evaluate the influence of deposition parameters on the electrodeposition of Cu–Co alloys in citrate medium. J Appl Electrochem. 2008;38(7):1763-9.
8. Al-Athel KS, Ibrahim M, Arif AFM, Akhtar SS. Effect of composition and thickness on the hardness and scratch resistance of copper and copper alloy coatings. Arab J Sci Eng. 2017;42(11):4895-904.
9. Lee WH, Chung KC. Investigation of a copper–nickel alloy resistor using coelectrodeposition. J Appl Electrochem. 2020;50(5):535-47.
10. Zhou NX, Silva PS, Braga AVC, do Lago DCB, Pimenta AR, Senna LF. Production of low-Sn Cu-Sn alloy coatings onto steel substrate using sodium citrate bath – part 1: the effect of current mode (DC or SPC) and applied current on the chemical, morphological, and anticorrosive properties of the coatings. Mater Res. 2022;25:e2022004.
11. Noce RD, Benedetti AV, Magnani M, Passamani EC, Kumar H, Cornejo DR, et al. Structural, morphological, and magnetic characterization of electrodeposited Co-Fe-W alloys. J Alloys Compd. 2014;611:243-8.
12. Casella I, Gatta M. Electrodeposition and characterization of nickel-copper alloy films as electrode material in alkaline media. J Electrochem Soc. 2002;149:B465.
13. Ghosh SK, Grover AK, Dey GK, Totlani MK. Nanocrystalline Ni–Cu alloy plating by pulse electrolysis. Surf Coat Tech. 2000;126(1):48-63.
14. Mohamed AE, Rashwan SM, Abdel-Wahaab SM, Kamel MM. Electrodeposition of Co–Cu alloy coatings from glycinate baths. J Appl Electrochem. 2003;33(11):1085-92.
15. Casella IG. Electrodeposition of cobalt oxide films from carbonate solutions containing Co(II)–tartrate complexes. J Electroanal Chem (Lausanne). 2002;520(1-2):119-25.
16. de Lima TG, Rocha BCCA, Braga AVC, do Lago DCB, Luna AS, Senna LF. Response surface modeling and voltammetric evaluation of Co-rich Cu–Co alloy coatings obtained from glycine baths. Surf Coat Tech. 2015;276:606-17.
17. Mebed AM. Two-phase Co–Cu thin films with size distribution of ferromagnetic nanostructures optimum for giant magnetoresistance. J Nanosci Nanotechnol. 2020;20(9):5686-92.
18. Jyoko Y, Kashiwabara S, Hayashi Y. Preparation of giant magnetoresistance Co-Cu heterogeneous alloys by electrodeposition. J Electrochem Soc. 1997;144(7):193-5.
19. Goranova D, Avdeev G, Rashkov R. Electrodeposition and characterization of Ni–Cu alloys. Surf Coat Tech. 2014;240:204-10.
20. Ladal J, Pingily A, Nallacheruvu GK. X-ray study of Cu30Ni70 alloy nanopowders prepared by ballmilling. Int J Eng Tech Res. 2014;2(2):188-92.
21. Shams El Din AM, El Dahshan ME, El Din Taj AM. Dissolution of copper and copper-nickel alloys in aerated dilute HCl solutions. Desalination. 2000;130(1):89-97.
22. Celis J, Cavallotti P, Silva J, Zielonka A. The future for electroplating electromagnetic materials in microelectronics. J Trans Inst Met Finish. 1998;76(5):163-70.
23. Song CH, Choi Y, Lee Y, Kim M. Electro-magnetic insulating behavior of thin multilayered copper-nickel composite mesh sheet formed by two-step pulse electroplating. Phys Met Metallogr. 2014;115(13):1275-80.
24. Mishra RS, Haridas RS, Agrawal P. High entropy alloys – tunability of deformation mechanisms through integration of compositional and microstructural domains. Mater Sci Eng A. 2021;812:141085.
25. Karahan H, Bakkaloglu OF, Bedi M. Giant magnetoresistance of electrodeposited Cu–Co–Ni alloy films. J Phys. 2007;68:83-90.
26. Pané S, Gómez E, Vallés E. Magnetoresistive granular Cu–Co–Ni coatings prepared by electrodeposition. J Electroanal Chem (Lausanne). 2006;596(2):87-94.
27. Karpuz A, Alper M, Kockar H. Microstructure dependence of magnetic properties on electrochemically produced ternary CuCoNi alloys. J Mater Sci Mater Electron. 2014;25:4483-8.
28. Mondal BN, Basumallick A, Chattopadhyay PP. Magnetic behavior of nanocrystalline Cu–Ni–Co alloys prepared by mechanical alloying and isothermal annealing. J Alloys Compd. 2008;457(1-2):10-4.
29. Curiotto S, Johnson E, Celegato F, Coisson M, Pryds N. Giant magnetoresistance in melt spun Cu85Co10Ni5. J Magn Magn Mater. 2009;321(3):131-6.
30. Kuo PC, Chen SY, Yu W, Okumura R, Iikubo S, Laksono AD, et al. The effect of increasing nickel content on the microstructure, hardness, and corrosion resistance of the $CuFeTiZrNi_x$ high-entropy alloys. Materials (Basel). 2022;15(9):3098.
31. Dong, Q, Jia, W, Zhang, Z, Zhang, D, Wu, J, Zhang, B. Effects of Ni content on the corrosion behavior of Al0.5CoCrFeNix high entropy alloys in acid and alkaline media. Mater Corros. 2022;73(8):1274-85.
32. Dai G, Wu S, Huang X. Preparation process for high-entropy alloy coatings based on electroless plating and thermal diffusion. J Alloys Compd. 2022;902:163736.
33. Fujiwara Y, Enomoto H. Electrodeposition of β-brass from cyanide baths with accumulative under potential deposition of Zn. J Electrochem Soc. 2000;147(5):1840-6.
34. Carlos IA, Bidoia ED, Pallone EMJA, Almeida MRH, Souza CAC. Effect of tartrate content on aging and deposition condition of copper–tin electrodeposits from a non-cyanide acid bath. Surf Coat Tech. 2002;157(1):14-8.
35. de Lima TG, Rocha BCCA, Braga AVC, do Lago DCB, Luna AS, Senna LF. Response surface modeling and voltammetric evaluation of Co-rich Cu–Co alloy coatings obtained from glycine baths. Surf Coat Tech. 2015;276:606-17.
36. Melo LC, Neto PL, Correia A. The influence of citrate and tartrate on the electrodeposition and surface morphology of Cu–Ni layers. J Appl Electrochem. 2011;41(4):415-22.
37. Deo Y, Guha S, Sarkar K, Mohanta P, Pradhan D. Mondal, Avik. Electrodeposited Ni-Cu alloy coatings on mild steel for enhanced corrosion properties. Appl Surf Sci. 2020;515:146078.

38. Hosseini MG, Ashassi-Sorkhabi H, Ghiasvand HAY. Electrochemical studies of Zn–Ni alloy coatings from non-cyanide alkaline bath containing tartrate as complexing agent. Surf Coat Tech. 2008;202(13):2897-904.
39. de Souza TM, do Lago DCB, Senna LF. Electrodeposition of Co-rich Cu-Co Alloys from Sodium Tartrate Baths Using Direct (DC) and Single Pulsed Current (SPC). Mater Res. 2019;22(3):e20180272.
40. Callister WD Jr. Materials science and engineering: an introduction. 7th ed. New York: John Wiley & Sons; 2007.
41. Cullity BD. Elements of X-rays diffraction. 2nd ed. London: Addison-Wesley; 1978.
42. Cano E, Lafuente D, Bastidas DM. Use of EIS for the evaluation of the protective properties of coatings for metallic cultural heritage: a review. J Solid State Electrochem. 2010;14:381-91.
43. Ballesteros J, Chainet E, Oziel P, Meas Y, Trejo G. Electrodeposition of Copper from Non-Cyanide Alkaline Solution Containing Tartrate. Int J Electrochem Sci. 2011;6:2632-51.
44. Brenner A. Electrodeposition of alloys. Vol. 2. New York: Academic Press; 1963.
45. Sasaki KY, Talbot JB. Electrodeposition of Binary Iron-Group Alloys. J Electrochem Soc. 1995;142:775-82.
46. Hessami S, Tobias CW. A mathematical model for anomalous co-deposition of nickel-iron on a rotating disk electrode. J Electrochem Soc. 1989;136(12):3611-6.
47. Zech N, Podlaha EJ, Landolt D. Rotating cylinder Hull cell study of anomalous co-deposition of binary iron-group alloys. J Appl Electrochem. 1998;28:1251-60.
48. Correia AN, Machado SAS. Electrodeposition and characterization of thin layers of Ni-Co alloys obtained from dilute chloride baths. Electrochim Acta. 2000;45(11):1733-40.
49. Gómez E, Ramirez J, Vallés E. Electrodeposition of Co-Ni alloys. J Appl Electrochem. 1998;28(1):71-9.
50. Jovic VD, Tošic N, Stojanović M. Characterization of electrodeposited Co + Ni alloys by application of the ALSV. J Electroanal Chem (Lausanne). 1997;420(1-2):43-51.
51. Budi S, Daud A, Radiman S, Umar A. Effective electrodeposition of Co–Ni–Cu alloys nanoparticles in the presence of alkyl polyglucoside surfactant. Appl Surf Sci. 2010;257(3):1027-33.
52. Sienna LF, Achete CA, Mattos OR, Hirsch T. Characterisation of PVD TiCN layers by physical and electrochemical methods. Surf Eng. 2005;21(2):144-50.
53. JCPDS: Joint Committee on Powder Diffraction Standards. Powder diffraction file — PDF-2 [CD-ROM]. Pennsylvania: ICDD; 2000.
54. Pattanaik GR, Pandya DK, Kashyap SC. Preparation of Cu-Co alloy thin films on n-Si by galvanostatic DC electrodeposition. J Electrochem Soc. 2002;149(7):C363-9.
55. Zhukova V, del Val JJ, Ilyn M, Ipatov M, Varga R, Garcia C, et al. GMR effect in Co-Cu microwires. J Korean Phys Soc. 2013;62(12):1940-4.
56. Sun, Z, Song, X, Hu, Z, Liang, G, Yang, S, Cochrane, RF. Effects of Ni addition on liquid phase separation of Cu–Co alloys. J Alloys Compd. 2001;319(1-2):276-9.
57. Yang J, Shen X, Ji Z, Zhou H, Zhu G, Chen K. In situ growth of hollow CuNi alloy nanoparticles on reduced graphene oxide nanosheets and their magnetic and catalytic properties. App Surf Sci, 2014;316:575-81.
58. Varea A, Pellicer E, Pané S, Nelson BJ, Suriñach S, Baró MD, et al. Mechanical properties and corrosion behaviour of nanostructured Cu-rich CuNi electrodeposited films. Int J Electrochem Sci. 2012;7:1288-302.
59. Zhang J, Wang Q, Wang Y, Wen L, Dong C. Highly corrosion-resistant Cu70 (Ni, Fe, Mn, Cr) 30 cupronickel designed using a cluster model for stable solid solutions. J Alloys Compd. 2010;505(1):179-82.
60. Thurber CR, Ahmad YH, Sanders SF, Al-Shenawa A, D'Souza N, Mohamed AM, et al. Electrodeposition of 70-30 Cu–Ni nanocomposite coatings for enhanced mechanical and corrosion properties. Curr Appl Phys. 2016;16(3):387-96.
61. Jagadale AD, Dubal DP, Lokhande CD. Electrochemical behavior of potentiodynamically deposited cobalt oxyhydroxide (CoOOH) thin films for supercapacitor application. Mater Res Bull. 2012;47(3):672-6.
62. Nuli YN, Zhang P, Guo ZP, Liu HK, Yang J. NiCo2O4/C nanocomposite as a highly reversible anode material for lithium-ion batteries. Electrochem Solid-State Lett. 2008;11(5):A64-7.
63. Gupta V, Gupta S, Miura N. Electrochemically synthesized nanocrystalline spinel thin film for high performance supercapacitor. J Power Sources. 2010;195(11):3757-60.
64. Karaagac O, Kockar H, Alper M, Haciismailoglu M. Influence of Co:Cu ratio on properties of Co–Cu films deposited at different conditions. J Magn Magn Mater. 2012;324(22):3834-8.
65. Qu NS, Zhu D, Chan KC, Lei WN. Pulse electrodeposition of nanocrystalline nickel using ultra narrow pulse width and high peak current density. Surf Coat Tech. 2003;168:123-8.
66. Li Y, Jiang H, Huang W, Tian H. Effects of peak current density on the mechanical properties of nanocrystalline Ni–Co alloys produced by pulse electrodeposition. Appl Surf Sci. 2008;254(21):6865-9.
67. Wang S, Guo X, Yang H, Dai J, Zhu R, Gong J, et al. Electrodeposition mechanism and characterization of Ni-Cu alloy coatings from a eutectic-based ionic liquid. Appl Surf Sci. 2014;288:530-6.
68. Subramanian B, Mohan S, Jayakrishnan S. Structural, microstructural and corrosion properties of brush plated copper–tin alloy coatings. Surf Coat Tech. 2006;201(3):1145-51.
69. Alexander CL, Tribollet B, Orazem ME. Contribution of surface distributions to constant-phase-element (CPE) behavior: 2. Capacitance. Electrochim Acta. 2016;188:566-73.
70. Robbiola L, Tran T, Dubot P, Majerus O, Rahmouni K. Characterisation of anodic layers on Cu–10Sn bronze (RDE) in aerated NaCl solution. Corros Sci. 2008;50(8):2205-15.